

## Technical Paper

# Flexural performance of sandwich panels utilizing high strength concrete, foam concrete and alkali-resistant glass fabric FRCM system

Kyung Chan Hong\*, Munkhtuvshin Ochirbud, Hosung Lee, Sangu Ha, Donguk Choi

(Received: October 21, 2024; Revised: December 27, 2024; Accepted: December 03, 2024; Published online: December 30, 2024)

**Abstract:** A new type of building sandwich panel was designed, fabricated, and tested. The sandwich panel used high strength concrete (HSC) for thin outer/inner sheets and foam concrete (FC) for the core insulation material, while both HSC sheets and the FC core were interconnected using alkali-resistant glass fabric (ARGF). The sandwich panel was designed using truss model. ARGF served two different purposes of (1) shear reinforcement and (2) flexural reinforcement. A total of seven sandwich panels were fabricated and tested under 3-point and 4-point flexural test. During the flexural test, the FC core first underwent gradual damage in the compression strut followed by development of multiple flexural cracks in the thin HSC sheet in or close to the constant moment zone under 4-point flexural test. As a result, the flexural test results of the sandwich panel showed pseudo-ductile behavior.

**Keywords:** Sandwich panel, High strength concrete, Foam concrete, Fabric reinforced cementitious matrix (FRCM), Recycled sand.

## 1. Introduction

COVID 19 that prevailed across globe was a big threat to humans. One phenomenon that occurred in South Korea during the COVID 19 pandemic period was increased number of distribution warehouses, which was needed due to increasing e-commerce. At the same time, number of fire accidents also increased in

the distribution warehouses across Korea due to easily flammable sandwich panels, which simply consisted of thin steel sheets and organic insulation (such as expanded polystyrene or polyurethane) bonded together. This type of conventional sandwich panels caught and spread fire easily. Therefore, it was deemed necessary to use sandwich panels which used inorganic components to decrease fatality due to fire in buildings including distribution warehouses.

\*Corresponding author **Kyung Chan Hong** is M.S. student of Dept. of Architectural Engineering, Hankyong National University, Anseong, South Korea. Email: [ghdrudcks96@hknu.ac.kr](mailto:ghdrudcks96@hknu.ac.kr)

**Munkhtuvshin Ochirbud** is a post-graduate researcher of Industry-Academy Cooperation Fund, Hankyong National University, Anseong, South Korea. Email: [tuvshin7616@hknu.ac.kr](mailto:tuvshin7616@hknu.ac.kr)

**Hosung Lee** is a CEO of Dongguk ENT Co. Ltd., Anseong, South Korea. Email: [vapersky@naver.com](mailto:vapersky@naver.com)

**Sangu Ha** is a Prof. of Division of Real Estate and Construction Engineering Kangnam University, Yongin, South Korea.

**Donguk Choi** is a NRF Research Prof. of Hankyong National University, Anseong, South Korea. Email: [choidu@hknu.ac.kr](mailto:choidu@hknu.ac.kr)

Many different types of commercial building sandwich panels are being used in practice, but most of them utilize organic insulation materials which can easily catch fire. Some researchers proposed different sandwich panel designs which used inorganic components. [3] investigated textile reinforced aerated concrete sandwich panels. Thin outer layers consisted of two layers of alkali-resistant glass textiles and a cementitious binder. Autoclaved aerated concrete and polypropylene fiber-reinforced aerated concrete were used as core insulation material. [5] developed and tested sandwich panels which combined thin layers of sisal-fiber cement composites and a core layer of fiber-reinforced lightweight concrete. The sandwich panels were fabricated by a cast hand-layup technique.

Lightweight aggregates and polypropylene fibers were used in the core concrete to reduce its density and post-cracking tensile strength. [11] proposed a sandwich panel which combined two layers of curioá fiber cement composites and a core layer of autoclaved aerated concrete (AAC) in a form of AAC block and evaluated flexural performance and the pull-off behavior between the cement composite and the AAC core.

Researchers also proposed other types of sandwich panels which not only used inorganic components but also shear reinforcement that connected the thin outer/inner sheets and the core to improve mechanical performance. [9] designed sandwich panels which consisted of two facings made of carbon reinforced textile reinforced concrete and a low density foamed concrete core. Glass fiber reinforced polymer (GFRP) connecting device was used to connect the facings and the core. [4] used reactive powder concrete with carbon textile reinforcement, i.e. textile reinforced reactive powder concrete, for thin outer layers and low-density foamed concrete as core material. Prefabricated GFRP connecting devices were used as shear connector. After experimental and analytical investigations using finite element analysis, they claimed that the structural behavior of the sandwich panels was highly dependent on the stiffness and strength of the connectors to ensure composite action.

This study was conducted to design and fabricate a new type of inorganic sandwich panel and evaluate its mechanical performance. Thin facings used high-strength concrete (HSC) with alkali-resistant glass fabric (ARGF) as flexural reinforcement, while the core material was lightweight foam concrete. ARGF was used not only as the flexural reinforcement, but also used as shear connector that connects thin outer/inner facings and the core. Flexural tests were performed on a total of seven sandwich panels and the mechanical performance was evaluated by four-point bending and three-point bending tests.

## 2. Material properties, fabrication of sandwich panel and test method

### 2.1. Material properties

Sandwich panels consisted of thin high strength concrete (HSC) sheets (thickness = ~10 mm) and foam concrete (FC) core insulation (thickness ~80 mm),

where the outer/inner thin HSC sheets and the FC core insulation were connected by alkali-resistant glass fabric (ARGF). ARGF was also used as flexural reinforcement in the thin HSC sheets.

#### 2.1.1. HSC

The high strength concrete (HSC) used ordinary Portland cement (OPC), silica fume (SF), fly ash (FA), and sand while the maximum particle size of sand was 2.5 mm. The mix proportion was determined using two-step packing density test methodology proposed by [8]. Binder: sand ratio was 3:7 by vol. and water-to-binder ratio (W/B) was 0.3. Natural crushed sand (NS) and recycled sand produced from waste concrete (RS) were used. Table 1 shows the mix proportion of the HSC. Polycarboxylate superplasticizer (1.5% of binder by mass) was used to control flow.

Table 1 – Mix proportion of HSC (unit: kg/m<sup>3</sup>)

OPC	SF	FA	NS/RS	W	SP	W/B
616	27.7	91.8	1,388	213	11.0	0.3

NOTE: NS:RS = 50:50 (by mass)

The HSC was cast using  $\phi$ 100 mm x 200 mm cylindrical mold, demolded after 24h, and then cured in a water pool until 28 days when the mechanical properties were tested. 28d compressive strength was 83.6 MPa. The elastic modulus was 30.0 GPa. Flexural strength which was tested using 100 mm x 100 mm x 400 mm prisms was 7.27 MPa.

#### 2.1.2. FC

The foam concrete (FC) was manufactured by chemical foaming method using hydrogen peroxide (H<sub>2</sub>O<sub>2</sub>, 35% diluted solution) as the foaming agent as H<sub>2</sub>O<sub>2</sub> decomposed into H<sub>2</sub>O and 1/2 O<sub>2</sub> in the highly alkaline environment of the fresh cementitious composite. HPMC was used as the foam stabilizer [6]. OPC, SF, and FA were used as binder materials and 100% RS was used as shown in Table 2. CaCl<sub>2</sub> (4.5% of binder by mass) was needed to accelerate the initial setting time of FC where the balance between the gravity of the constituents, the foaming pressure, and the resistance of the matrix with high early strength against foam collapse was important. 12-mm polypropylene

Table 2 – Mix proportion of FC (kg/m<sup>3</sup>)

OPC	SF	Fly ash	W	RS	SP	CaCl <sub>2</sub>	pp	H <sub>2</sub> O <sub>2</sub>	HPMC
473	29.6	88.7	411	887	11.8	26.6	4.56	29.6	0.9

NOTE: HPMC - hydroxypropyl methylcellulose ether

Table 3 – Physical and mechanical properties of FC

SSD density (kg/m <sup>3</sup> )	OD density (kg/m <sup>3</sup> )	Water absorption (%)	28d compressive strength (MPa)	Elastic modulus (MPa)	Thermal conductivity (W/m-K)
1,199	525	56.2	0.82	23.4	0.109

fiber (pp, 0.5% by vol.) was used to improve the flexural strength of FC. Melamine-base SP (2% of binder by mass) was used to increase flow.

The FC was cast and cured under PE film for 7 days and then cured in room condition until 28 days of age when the mechanical properties were tested. 300 mm x 300 mm x 50 mm FC panel specimens were oven dried for 7 days, and oven dry mass ( $W_{OD}$ ) was measured. The same specimen was then soaked in water for another 7 days. The specimen was retrieved and the surface water was removed using dry towels and the surface saturated dry mass ( $W_{SSD}$ ) was measured. The water absorption was determined using Eq. (1). 100 mm x 100 mm x 100 mm cubes were used to determine compressive strength, which is 0.81 MPa in Table 3. The physical and mechanical properties of FC are summarized in Table 3. The thermal conductivity was measured by hot plate method following KS F 2463:2019. Thermal conductivity is 0.109 W/mK as shown in Table 3.

$$water\ absorption = \frac{W_{SSD} - W_{OD}}{\rho_w W_{SSD}} \times 100 \quad (1)$$

where  $\rho_w$  is specific gravity of water.

### 2.1.3. ARGF

The alkali-resistant glass fabric (ARGF) was a commercial two-way mesh. The axial fiber roving (warp) has cross-sectional area twice that of the transverse fiber roving (weft) as shown in Table 4. The tensile properties of the ARGF were tested using 50-kN tensile testing machine. The ARGF showed linearly-elastic behavior up to failure in tension, while the tensile strength is 941 MPa and the elastic modulus is 41.6 GPa as shown in Table 4.

Table 4 – Mechanical properties of ARGF

Strength, $f_{fu}$ (MPa)	Strain at peak, $\epsilon@f_{fu}$ (%)	Elastic modulus, Ef (GPa)
941	2.27	41.62

NOTE: Cross-sectional area of warp = 0.221 mm<sup>2</sup> per roving; cross-sectional area of weft = 0.113 mm<sup>2</sup> per roving

## 2.2. Fabrication of sandwich panel

Fig. 1 schematically shows the fabrication procedure where ARGF was installed as shear reinforcement in all sandwich panels tested. ARGF was also utilized as the flexural reinforcement in Stage II test specimens. A sandwich panel was fabricated in the following sequence (See Fig. 1):

1. FC core casting;
2. Removal of excess FC;
3. 1<sup>st</sup> HSC sheet casting on top of FC;
4. 2<sup>nd</sup> HSC sheet casting.

## 2.3. Test methods of sandwich panels

A total of seven sandwich panels was fabricated and tested under flexure in two different Stages. In Stage I, three 240 mm ( $B$ ) x 500 mm ( $L$ ) x ~100 mm ( $H$ ) sandwich panels were tested under 4-point bending. In Stage I, ARGF was used only as shear reinforcement (i.e. the thin HSC sheets did not include the ARGF as flexural reinforcement). In Stage II, four sandwich panels with the dimensions the same as Stage-I test specimens were fabricated while two panels were tested under 3-point bending and two other panels were tested under 4-point bending. In Stage II, ARGF

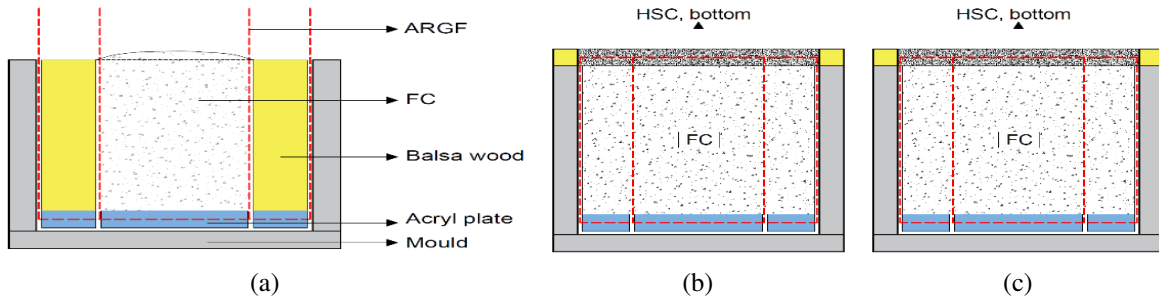


Fig. 1 – Casting sequence of a sandwich panel (not to scale)

was used both as the shear reinforcement and the flexural reinforcement: i.e. thin HSC sheets included one layer of ARGF flexural reinforcement. Table 5 summarizes the flexural test specimens.

Table 5 – Summary of flexural test specimens and test variables

Stage	Index	Dimensions (mm)					$\rho_f$ (%)	Test method	
		$B$	$t_{ts}$	$t_{bs}$	$t_c$	$H$			
I	B6-1	240	11.3	10.5	79.3	101	500	0.074	4p
	B6-3	240	6.7	7.7	80.0	94.4	500	0.074	4p
	B6-4	240	6.0	7.0	77.0	90.0	500	0.074	4p
II	MB6-1	240	8.2	9.4	76.7	94.3	500	0.074	4p
	MB6-2	240	9.2	7.8	76.4	93.5	500	0.074	4p
	MB6-3	240	10.8	12.5	69.8	93.2	500	0.074	3p
	MB6-4	240	11.1	12.0	72.6	95.7	500	0.074	3p

NOTE:  $t_{ts}$  – thickness of top sheet;  $t_{bs}$  – thickness of bottom sheet;  $t_c$  – thickness of FC core; 4p – four-point bending (third points bending); 3p – three-point bending

### 2.3.1. Flexural test, Stage I

Three sandwich panels were tested under 4-point bending. In Table 5, the shear reinforcement ratio  $\rho_f$  was defined as the volumetric ratio of the fabric (warp) over total volume of the panel as shown in Eq. (2).  $\rho_f$  was 0.074% for all specimens.

$$\rho_f = \frac{A_f H}{B H_s} \times 100\% \quad (2)$$

where  $A_f$  is total cross-sectional area of vertical ARGF rovings (warp,  $\text{mm}^2$ ) within distance equal to center-to-center spacing  $s$  between adjacent ARGFs (mm),  $B$  is width of panel (mm),  $H$  is height of panel (mm)

### 2.3.2. Flexural test, Stage II

A total of four sandwich panels was tested: two specimens under 4-point bending and two specimens under 3-point bending. The shear reinforcement ratio  $\rho_f$  was 0.074% for all specimens. In Stage II tests,

ARGF were used both as flexural reinforcement as well as shear reinforcement. The flexural reinforcement ratio was defined as the ratio of cross-sectional area of ARGF (warp) over cross-sectional area of thin HSC sheet and was 0.44%.

### 2.3.3. Test method

For the 4-point bending test, the point loads were applied at one-third locations. Span length was 480 mm. Displacement at center was measured using two linear variable displacement transducers (LVDTs) as shown in Fig. 2. For the 3-point bending test, the point load was applied at center and the displacement at center was measured using two LVDTs. A compression test machine of 2,500-kN capacity was used under displacement control with the ramp speed of 0.1 mm/m.

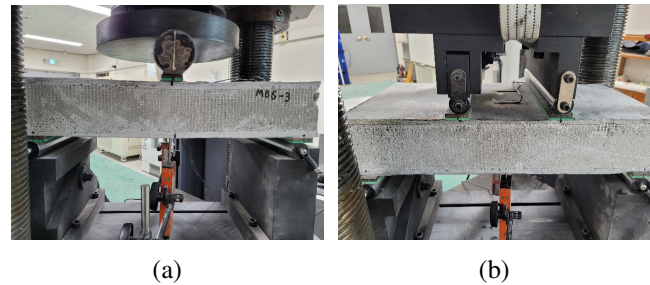


Fig. 2 – Flexural test under progress (4-point bending)

### 2.4. Truss model

Fig. 3 shows a truss model of the sandwich panel. The compression chord and the tension chord are the HSC thin sheets and the core is FC while the HSC thin sheets and the FC core are vertically connected by ARGF so that ARGF works as the shear reinforcement in a reinforced concrete beam in this model. Table 6 summarizes the results of truss analysis. Results of the truss analysis summarized in Table 6 shows the

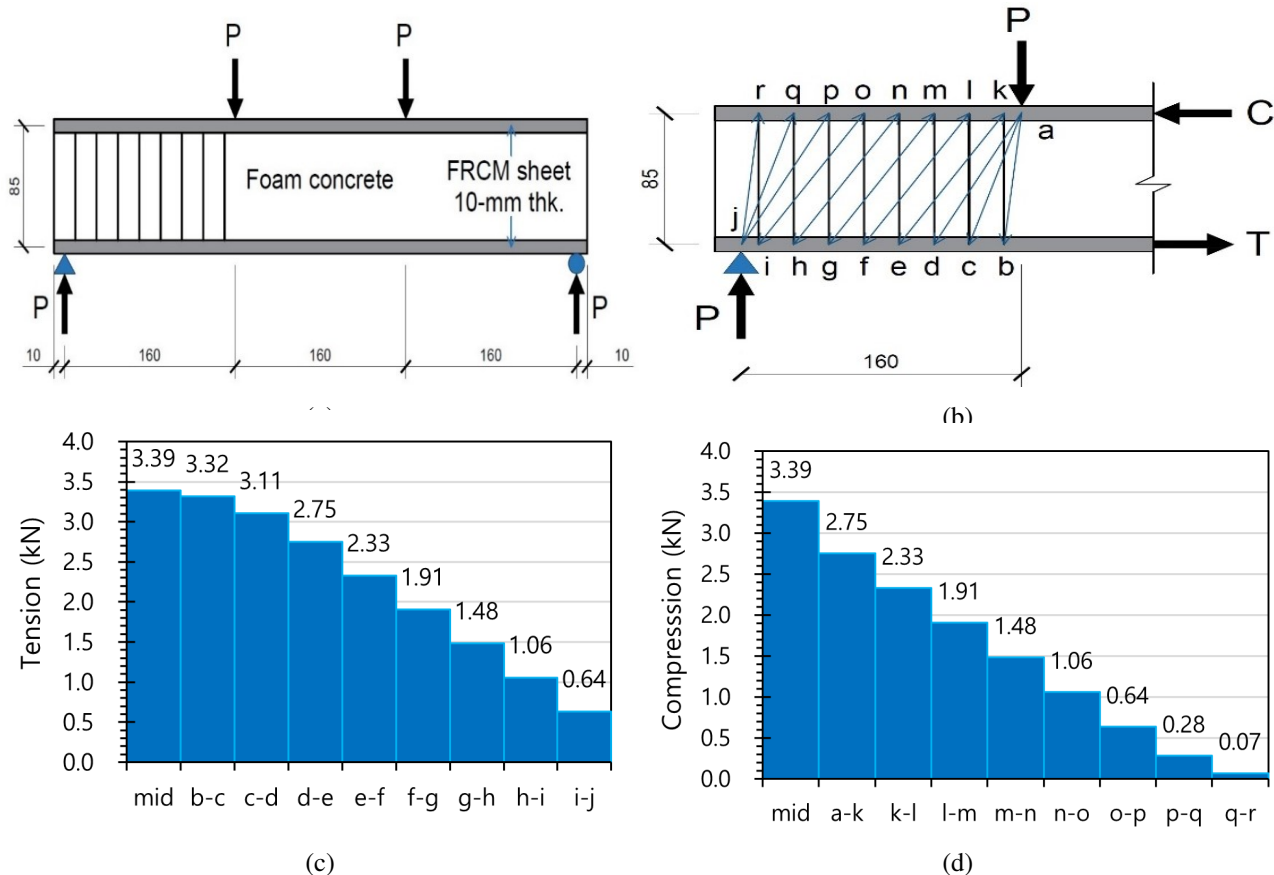


Fig. 3 – Truss model of sandwich panel

following:

Table 6 – Results of truss analysis:  $P = 1.8 \text{ kN}$ ,  $\rho_f = 0.074\%$

Force	Compression sheet	Tension sheet	Core concrete	Remarks
(1) Acting	1.41 MPa	1.41 MPa	0.19 MPa	Diagonal compression failure of FC governs
(2) Capacity	83.6 MPa	7.27 MPa	0.76 MPa	
(1)/(2) * 100	2.05%	18.3%	25.0%	

- When  $P = 1.8 \text{ kN}$  (or  $2P = 3.6 \text{ kN}$ ), the compressive stress in the top plate is 1.41 MPa (or 2.1% of capacity), tensile stress in the bottom plate is 1.41 MPa (or 18.3% of capacity), and diagonal compressive stress in the FC core is 0.19 MPa (or 25% of capacity).
- Therefore, as  $P$  increases, the FC is the component where the failure will initiate (i.e. FC failure under compression), which will be followed by tensile failure of the bottom plate.

### 3. Flexural test results

#### 3.1. Stage-I flexural test results

Three sandwich panel specimens were tested under 4-point bending in Stage I. Table 7 summarizes the Stage-I flexural test results. Load-vs-displacement plots of three Stage-I test specimens are shown in Fig. 4. In Fig. 4, the displacement increases in proportion to increasing load until the load reaches about 5.3~5.7 kN, where the load decreases a little and then increases again. After this point, the stiffness is reduced slightly, but the displacement keeps increasing almost linearly with increasing load until the peak load. In Fig. 4, the linearly-elastic part of the load-vs-displacement plot between the origin and the point the stiffness begins to decrease is where the compressive crushing of the FC core begins to occur as predicted by the truss model (See 2.4). Fig. 4 also shows that the part of the load-vs-displacement plots between the initiation of the FC crushing and the peak load includes small multiple ups and downs of load in the load-vs-displacement plots

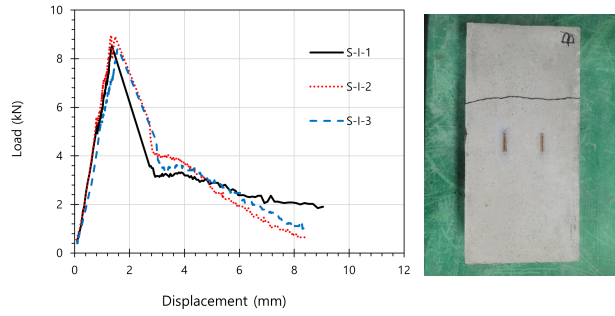


Fig. 4 – Load-vs-displacement plot of flexural test: Stage I (No ARGF flexural reinforcement)

Table 7 – Summary of Stage-I flexural test results (4-point bending)

Index	FC initial failure		Peak load	
	Load (kN)	Displ. (mm)	Load (kN)	Displ. (mm)
S-I-1	5.33	0.72	8.52	1.26
S-I-2	5.60	0.69	8.91	1.23
S-I-3	5.72	0.94	8.42	1.49

which indicate continuing damage of the FC core after the initial crushing. At the peak load, a flexural crack forms in the bottom HSC sheet, and the load decreases fast with fast increasing displacement. Final failure occurred with cracking/crushing in the thin compression sheet. Brittle failure was observed in Stage-I flexural test, where the thin HSC sheet did not include ARGF flexural reinforcement. The maximum load of the Stage I test specimen is 8.4-8.9 kN, and the deflection at center is 1.2-1.5 mm in Table 7.

### 3.2. Stage-II flexural test results

#### 3.2.1. 4-point bending

Two sandwich panel specimens were tested under 4-point bending: S-II-1 and S-II-2. Table 8 summarizes all Stage-II test results. Fig. 5 shows load-vs-displacement plots of two specimens tested under 4-point bending. In Fig. 5, displacement increases in proportion to increasing load until the load reaches about 5.4 kN, where the load decreases a little and then increases again. After this point, the stiffness is slightly reduced, but the displacement keeps increasing linearly with increasing load until the cracking load, which is reached at 9.6~10.7 kN. Load further increases and the peak load is reached at 11.5~12.6 kN with displacement of 3.6~4.9 mm at the peak. Fig. 5 shows that

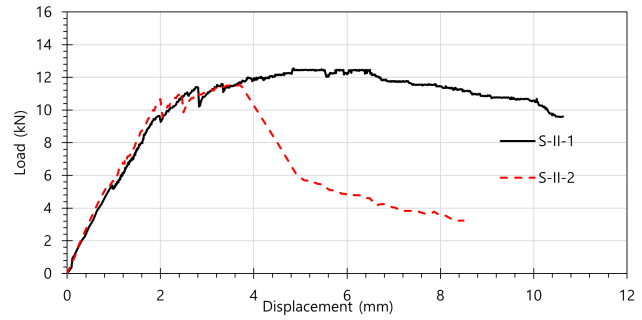


Fig. 5 – Load-vs-displacement plot of Stage-II flexural test under 4-point bending

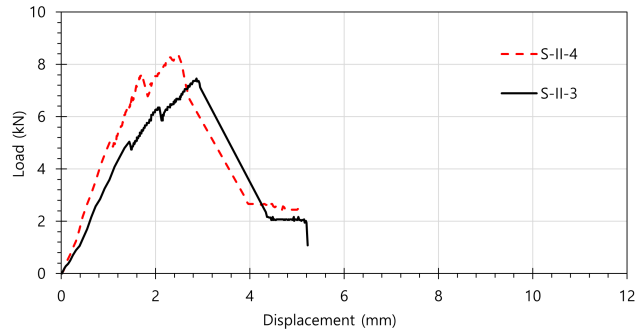


Fig. 6 – Load-vs-displacement plot of Stage-II flexural test under 3-point bending

the ascending curve of the load-vs-displacement plot consists of three parts: (1) origin-first FC crushing, (2) first FC crushing-first cracking, (3) first cracking-peak load. After the peak, the behavior is a little different between two specimens. For S-II-1, load slowly decreases with increasing displacement, because the bottom HSC sheet developed multiple cracks in the ARGF FRCM as shown in Fig. 9(a), (b) as well as Fig. 8(a), (b). For S-II-2, load rather abruptly decreases after the peak. This is because only two flexural cracks first developed in the bottom sheet which, as inclined cracks, progressed toward the loading points in the top sheet as shown in Fig. 8(c), (d). This resulted in a flexural failure with limited ductility. In both tests, the overall load-vs-displacement plots show more ductile behavior due to three-part ascending behavior, which is different from the behavior of the Stage-I test specimens. This is because of the use of additional flexural reinforcement in the thin outer sheet (HSC tensile sheet) in a form of ARGF while the ductile behavior is demonstrated by multiple cracking (See Fig. 7(a), (b)).

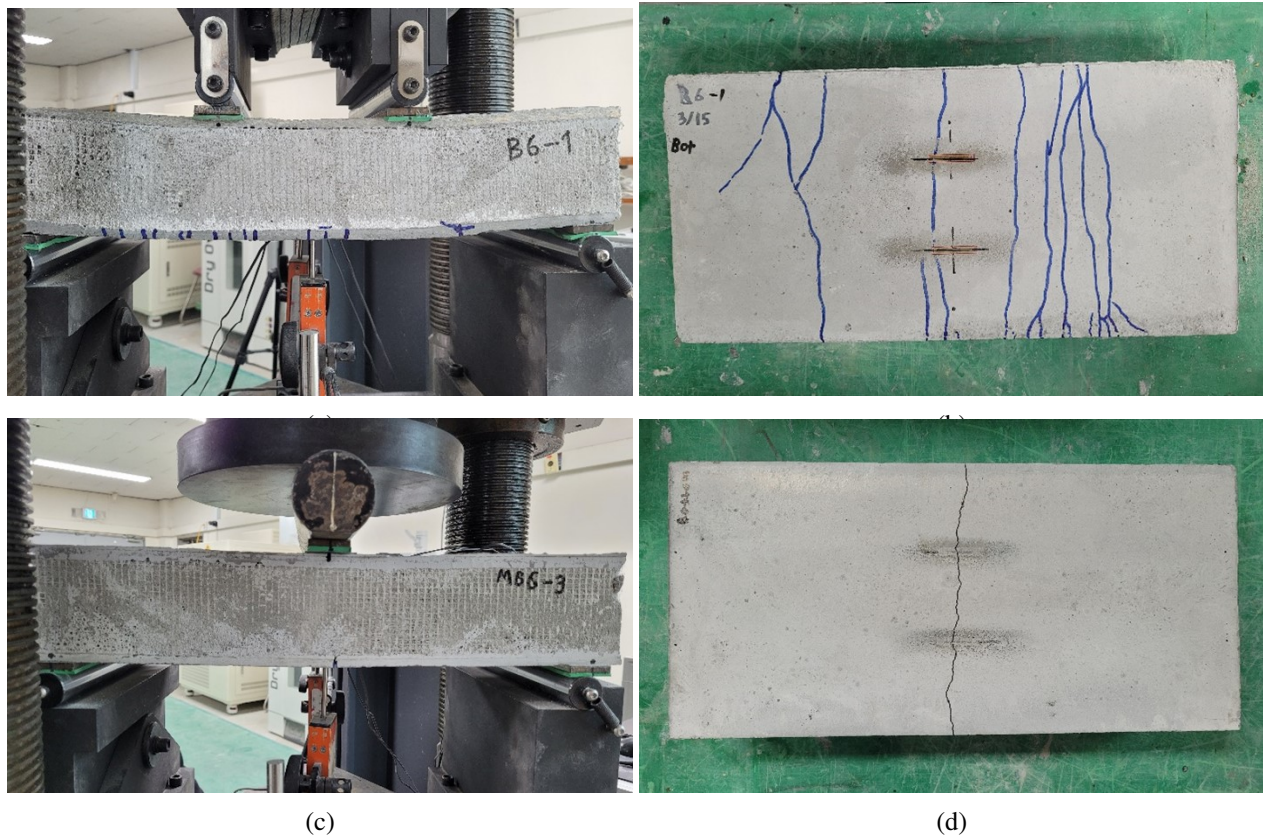


Fig. 7 – Test results under 4-point and 3-point bending: S-II-1 (4P) & S-II-3 (3P)

Table 8 – Summary of Stage-I flexural test results (4-point bending)

Index	FC initial failure		First cracking		Peak load		Test method
	Load (kN)	Displ. (mm)	Load (kN)	Displ. (mm)	Load (kN)	Displ. (mm)	
S-II-1	5.39	1.03	9.63	1.95	12.6	4.86	4P
S-II-2	5.36	0.92	10.7	2.00	11.5	3.62	4P
S-II-3	5.08	1.57	6.35	2.08	7.46	2.87	3P
S-II-4	4.98	1.12	7.65	1.71	8.36	2.49	3P

NOPT: 4P – 4-point bending; 3P – 3-point bending

### 3.2.2. 3-point bending

Table 8 also includes test results of two Stage-II specimens tested under 3-point bending. Fig. 6 shows the load-vs-displacement plots of two specimens: S-II-3 and S-II-4. The behavior in the ascending part is similar to that of the Stage-II specimens tested under 4-point bending as the ascending curve consists of three parts: (1) origin-first FC crushing, (2) first FC crushing-first cracking, (3) first cracking-peak load. Load at the first FC core crushing is 5.0~5.1 kN, the first cracking load is 6.4~7.7 kN, and the peak load is 7.5~8.4 kN. In Table 8, Fig. 5, and Fig. 6, the peak load of the specimens

tested under 3-point bending is lower than that of the specimens tested under 4-point bending due to longer span and increased moment. Both specimens developed single flexural crack at center at the peak load, and immediately lost resistance. Fig. 7 shows photos of S-II-1 (4-point bending) and S-II-3 (3-point bending).

### 3.2.3. Crack pattern

Cracks developed on the side face of the sandwich panels were investigated after removing ARGF meshes after completion of test. The crack patterns developed in the sandwich panels subjected to 4-point bending

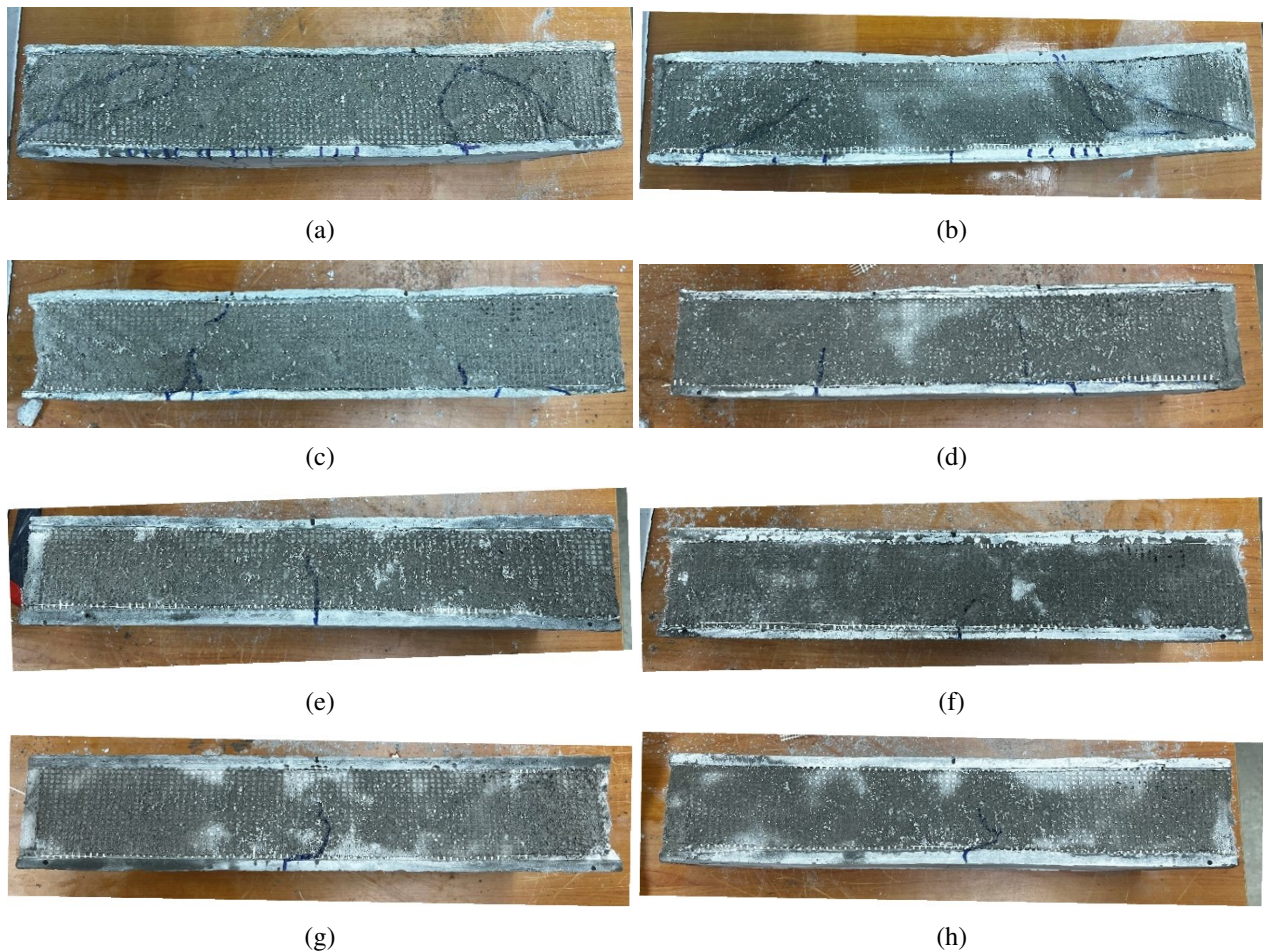


Fig. 8 – Cracks developed on side faces

are different from those of the sandwich panels tested under 3-point bending in Fig. 8. In Fig. 8(a), multiple flexural cracks develop in the bottom HSC sheet. At least one flexural crack further develops into FC core insulation. In addition, shear cracks also develop in the FC core including debonding between the FC core and the bottom HSC sheet (See Fig. 8(b)) and the web shear cracks for S-II-1. For S-II-2, two flexural cracks first developed in the thin HSC sheet further develop into FC core as shown in Fig. 8(c) and (d). At least one flexural crack reaches the top HSC sheet and the final failure occurs by cracking/partial crushing of the top sheet. On the other hand, in both sandwich panels tested under 3-point bending, a flexural crack occurs in the middle at bottom HSC sheet and the flexural crack further develops into FC core, which leads to flexural failure of both specimens: S-II-3 and S-II-4 as shown in Fig. 8(e)~(h).

## 4. Discussions

### 4.1. Modelling of load-vs-displacement behavior

Test results of Stage-II specimens tested under 4-point bending and 3-point bending reveal that the ascending part of the load-vs-displacement plot can be modeled using a tri-linear curve as shown in Fig. 9.

1. O-A – origin-first crushing of FC core insulation
2. A-B – first crushing of FC core insulation-first cracking of HSC sheet
3. B-C – fist cracking of HSC sheet-peak load

### 4.2. Analysis of displacement

It is noted that the displacement at center of the sandwich beams consists of two parts: (1) displacement

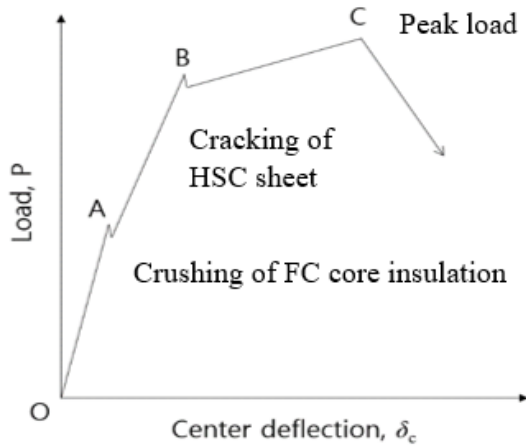


Fig. 9 – Tri-linear model of ascending part followed by a descending part of load-displacement behavior

due to bending moment and (2) displacement due to shear force. Structural mechanics provide Eqs. (3) and (4) as relationship of load and displacement at center under 4-point bending and 3-point bending, respectively [1].

$$\delta_c = \frac{236Pl^3}{1296EI} + \frac{Pl}{6GA} \quad (3)$$

$$\delta_c = \frac{Pl^3}{48EI} + \frac{Pl}{4GA} \quad (4)$$

where P is total applied load,  $\delta_c$  is vertical deflection at center, l is span length, EI is flexural stiffness, and GA is shear stiffness.

Eqs. (3) and (4) can be rewritten as Eqs. (5) and (6) where  $D = EI$  and  $U = GA$ . Stiffness of the sandwich panel can be determined by solving a set of simultaneous equations with two unknowns D and U using the test data on load and deflection at center [10].

$$\frac{\delta_c}{Pl} = \frac{236l^2}{1296D} + \frac{1}{6U} \quad (5)$$

$$\frac{\delta_c}{Pl} = \frac{l^2}{48D} + \frac{1}{4U} \quad (6)$$

Table 9 summarizes change of stiffnesses in the three-part ascending curve of the sandwich panel. Table 9 shows that D (flexural stiffness) is largest in the beginning and then decreases a little after crushing of the FC core. After the first cracking, D decreases significantly as the bottom HSC sheet does not provide resistance while only the ARGF flexural reinforcement resists the tension after cracking. U (shear stiffness) shows the same trend as D, although D increases a little

Table 9 – Stiffness of sandwich panel (unit:  $D, N \cdot mm^2$ ;  $U, N$ )

Stiffness	O-A	O-B	O-C
$D$	$3.25 \times 10^{10}$	$2.95 \times 10^{10}$	$0.71 \times 10^{10}$
$U$	$1.86 \times 10^6$	$2.52 \times 10^6$	$0.95 \times 10^6$

Table 10 – Analysis of deflections

Test type	A		B		C	
	flexure	shear	flexure	shear	flexure	shear
4-P bending	53.4%	46.7%	51.1%	48.9%	74.2%	25.8%
3-P bending	49.2%	50.8%	31.6%	68.4%	69.3%	30.7%

after FC crushing and then decreases fast after cracking as shown in Table 10. The reason U increases and then decreases is not clear, but it may be due to insufficient number of test data. Eqs. (3) and 4 can be used to determine the deflection at center caused by flexure and shear, respectively. Table 10 shows the contribution of both bending moment and shear force on the center deflection. For the two sandwich beams subjected to 4-point bending, the deflection at center due to flexure and shear is about the same when the FC core crushes and when the first cracking occurs. After the cracking, the deflection by flexure dominates as summarized in Table 10. Above results show that the shear behavior is important for the sandwich beams where the stiffness of the core insulation is very small. For the two sandwich beams subjected to 3-point bending, the contribution of flexure and shear is again about the same when the FC core first crushes. After the first cracking, the deflection by flexure dominates as shown in Table 10.

## 5. Conclusions

New type of sandwich panel which consists of inorganic components were designed, fabricated, and tested. High strength concrete (HSC), foam concrete (FC), and alkali-resistant glass fabric (ARGF) were constituted the sandwich panel, while the ARGF interconnected thin HSC outer/inner sheets and FC core insulation. ARGF was also used as flexural reinforcement of the thin HSC sheet: i.e. thin HSC sheet with ARGF formed ARGF fabric reinforced cementitious matrix (FRCM) for the panel. The findings can be summarized as follows:

1. Truss model was used to proportion each

component of the sandwich panel. The results of the truss panel analysis predicted that the failure under flexure begins by collapse of the FC in the compression strut followed by cracking of the tensile HSC sheet, which was corroborated by test;

2. Sandwich panel was tested under both 3-point and 4-point flexural test. 4-point flexural test results showed pseudo-ductile behavior of the sandwich panel in the ascending curve, which can be modeled using a tri-linear model;
3. Results of 3-point and 4-point flexural tests were used to analytically determine the flexural stiffness and the shear stiffness of the sandwich panel. Analysis results show that the stiffness of the sandwich panel is almost maintained until the first cracking of the panel, but then decreases fast after cracking;
4. Results of the deflection analyses show that the deflection is due to both flexural deformation and shear deformation while the contribution of the flexural and the shear deformation is almost the same up to the first cracking. After the first cracking, the deflection by the flexural deformation governs.

### Acknowledgement

This research was supported by Global Infrastructure Program through the National Research Foundation of Korea (NRF) funded by the Ministry of Science and ICT (grant number: 2021K1A3A1A20001722). Authors appreciate generous funding provided by National Research Foundation of South Korea.

### References

- [1] Allen, H. G. (1969). *Analysis and Design of Structural Sandwich Panels*. Pergamon Press.
- [2] ACI 549.4R-20. (2020). *Guide to Design and Construction of Externally Bonded Fabric-Reinforced Cementitious Matrix and Steel-Reinforced Grout Systems for Repair and Strengthening of Concrete Structures*. American Concrete Institute. Detroit, Michigan.
- [3] Dey, V., Zani, G., Colombo, M., Di Prisco, M., & Mobasher, B. (2015). Flexural impact response of textile-reinforced aerated concrete sandwich panels. *Materials and Design*, 86, 187–197.
- [4] Fransbjer, M., Portal, N. W., Vennetti, D., & Mueller, U. (2018). Composite Behaviour of Textile Reinforced Reactive Powder Concrete Sandwich Façade Elements. *International Journal of Concrete Structures and Materials*, 12, 71.
- [5] Frazão, C., Barros, J., Toledo Filho, R., Ferreira, S., & Goncalves, D. (2018). Development of sandwich panels combining Sisal Fiber-Cement Composites and Fiber-Reinforced Lightweight Concrete. *Cement and Concrete Composites*, 86, 206–223.
- [6] Ochirbud, M., Hong, K., Kang, S., Kim, Y., Ha, S., & Choi, D. (2022). Ultra-light foamed concrete with recycled sand. *Journal of Asian Concrete Federation*, 8(2), 23–34.
- [7] KS F 2463. (2019). *Standard test method of thermal conductivity for materials by means of the guarded hot plate*. Guacheon, Korea.
- [8] Kwan, A. H. K., & Fung, W. W. S. (2009). Packing density measurement and modeling of fine aggregate and mortar. *Cement & Concrete Composites*, 31, 349–357.
- [9] Portal, N. W., Flansbjer, M., Zandi, K., Wlasak, L., & Malaga, K. (2017). Bending behaviour of novel Textile Reinforced Concrete-foamed concrete (TRC-FC) sandwich elements. *Composite Structures*, 177, 104–118.
- [10] Reis, E. M., & Rizkalla, S. H. (2008). Mechanical characteristics of 3-D FRP sandwich panels. *Construction and Building Materials*, 22, 1009–1018.
- [11] Salgado, I. P., & Silva, F. A. (2021). Flexural behavior of sandwich panels combining curaua fiber-reinforced composite layers and autoclaved aerated concrete core. *Construction and Building Materials*, 86, 122890.